Dalton Transactions

Gamma radiolysis of hydrophilic diglycolamide ligands in concentrated aqueous nitrate solution

Journal:	*Dalton Transactions*
Manuscript ID	DT-ART-10-2019-003918.R1
Article Type:	Paper
Date Submitted by the Author:	22-Oct-2019
Complete List of Authors:	Horne, Gregory; Idaho National Laboratory, Center for Radiation Chemistry Research Wilden, Andreas; Forschungszentrum Jülich GmbH, IEK-6 Mezyk, Stephen; California State University at Long Beach, Chemistry and Biochemistry Twight, Liam; California State University Long Beach, Chemistry and Biochemistry Hupert, Michelle; Research Center Jülich, Central Institute for Engineering, Electronics and Analytics (ZEA-3) Stark, Andrea; Forschungszentrum Jülich GmbH, Zentralinstitut für Engineering, Elektronik und Analytik (ZEA-3) Verboom, Willem; University of Twente, Laboratory of Molecular Nanofabrication Mincher, Bruce; Idaho National Laboratory, Aqueous Separations and Radiochemistry Modolo, Giuseppe; Forschungszentrum Juelich GmbH,

Dalton Transactions ARTICLE

Gamma radiolysis of hydrophilic diglycolamide ligands in concentrated aqueous nitrate solution

Received 00th September 2019,
Accepted 00th November 2019

DOI: 10.1039/x0xx00000x

Gregory P. Horne,*[a] Andreas Wilden,*[b] Stephen P. Mezyk,[c] Liam Twight,[c] Michelle Hupert,[d] Andrea Stärk,[d] Willem Verboom,[e] Bruce J. Mincher,[a] and Giuseppe Modolo[b]

The radiation chemistry of a series of hydrophilic diglycolamides (DGAs: TEDGA, Me-TEDGA, Me_2-TEDGA, and TPDGA) has been investigated under neutral pH, concentrated, aqueous nitrate solution conditions. A combination of steady-state gamma and time-resolved pulsed electron irradiation experiments, supported by advanced analytical techniques and multi-scale modeling calculations, have demonstrated that: (i) the investigated hydrophilic DGAs undergo first-order decay with an average dose constant of (-3.18 ± 0.23) × 10^{-6} Gy^{-1}; (ii) their degradation product distributions are similar to those under pure water conditions, except for the appearance of NO_x adducts; and (iii) radiolysis is driven by hydroxyl and nitrate radical oxidation chemistry moderated by secondary degradation product scavenging reactions. Overall, the radiolysis of hydrophilic DGAs in concentrated, aqueous nitrate solutions is significantly slower and less structurally sensitive than under pure water conditions, similar to their lipophilic analogs. Overall, acid hydrolysis, not radiolysis, is expected to limit their useful lifetime. These findings are promising for the deployment of hydrophilic DGAs as actinide aqueous phase stripping and hold-back agents, due to the presence of high concetrations of nitrate in envisioned large-scale process conditions.

Introduction

Lipophilic diglycolamides (DGAs) have been extensively studied as trivalent actinide (An(III)) and lanthanide (Ln(III)) extractants for application in spent nuclear fuel reprocessing and recycling scenarios.[1-3] These molecules are structurally flexible, exhibit relatively high affinities for An(III), and fulfil the CHON principle – being composed of only carbon, hydrogen, oxygen, and nitrogen elements – which is beneficial as it enables incineration of waste without the generation of secondary waste streams.[4] Their structural versatility has led to the synthesis of a range of hydrophilic DGA derivatives, such as *N*,*N*,*N*′,*N*′-tetramethyldiglycolamide (TMDGA) and *N*,*N*,*N*′,*N*′-tetraethyldiglycolamide (TEDGA) shown in Fig. 1.

Many of these derivatives have been shown to be successful aqueous phase stripping[5-7] and hold-back agents.[8-11] However, their potential for application as aqueous phase actinide complexants is hindered by a limited understanding of their radiolytic behaviour and the impact of their degradation products on separation process performance. Actinide complexants are exposed to a multi-component radiation field that induces their radiolysis and degradation product formation. While the radiation chemistry of the lipophilic DGAs has been well characterized,[12-15] to date only a single experimental investigation has explored the radiation chemistry of the hydrophilic DGAs.[16] Koubský *et al.* studied hydrophilic DGAs using computational methods and confirmed the experimentally observed trend in radiolytic stability with increasing molecular weight.[17] Wilden *et al.* reported on the radiolytic and hydrolytic degradation of a series of hydrophilic DGAs under *pure water conditions*.[16] Despite the formation of similar degradation product distributions, the hydrophilic DGAs were much more susceptible to radiolysis compared to their lipophilic analogues. For example, the dose constant[18] (*d*) for TMDGA (*d* = (-14.9 ± 1.2) × 10^{-6} Gy^{-1})[16] is considerably larger than the equivalent for TODGA (*d* = (-4.1 ± 0.3) × 10^{-6} Gy^{-1})[12,14]. These observations were rationalized by reaction kinetics measurements highlighting the affinity of the hydrophilic DGAs for the highly oxidizing hydroxyl radical (•OH, E^o = 2.7 V) from water radiolysis:[19]

$$H_2O \rightsquigarrow [0.28]^{\bullet}OH + [0.06]H^{\bullet} + [0.27]e_{aq}^{-} + [0.05]H_2 + [0.07]H_2O_2 + [0.27]H_{aq}^{+}, \quad (1)$$

where the numbers in brackets are the radiolytic yields of deposited energy (*G*-values in μmol J^{-1}) for species production. For example, the rate coefficient (*k*) for the reaction of TEDGA with the •OH is very fast, *k*(TEDGA + •OH) = (2.91 ± 0.10) × 10^9 M^{-1} s^{-1}.[16] The lipophilic DGAs have been shown to react with the organic phase equivalent of the •OH, the organic radical cation ($R^{\bullet+}$), at similar diffusion limited rates, *k*(TODGA + $R^{\bullet+}$) = (9.72 ± 0.10) × 10^9 M^{-1} s^{-1}.[12] However, lifetimes of these organic transients are typically far shorter than that of the •OH, making them less available to induce DGA radiolysis. For example, the *n*-dodecane radical cation undergoes rapid ion-recombination within ~2 ns,[20] while the •OH is typically still available for reaction at microsecond timescales in pure water.

[a] Idaho National Laboratory, Center for Radiation Chemistry Research, Idaho Falls, ID, P.O. Box 1625, 83415, USA
[b] Forschungszentrum Jülich GmbH, Institut für Energie- und Klimaforschung – Nukleare Entsorgung und Reaktorsicherheit (IEK-6), 52428 Jülich, Germany.
[c] California State University Long Beach, Department of Chemistry and Biochemistry, Long Beach, CA 90804.
[d] Forschungszentrum Jülich GmbH, Zentralinstitut für Engineering, Elektronik und Analytik (ZEA-3), 52428 Jülich, Germany.
[e] University of Twente, Mesa+ Institute for Nanotechnology, Laboratory of Molecular Nanofabrication, P.O. Box 217, 7500 AE Enschede, The Netherlands.
*E-mails: gregory.p.horne@inl.gov and a.wilden@fz-juelich.de.
† Electronic Supplementary Information (ESI) available: HPLC-ESI-MS/MS solvent gradients, reaction kinetics figures, and degradation product tables. See DOI: 10.1039/x0xx00000x

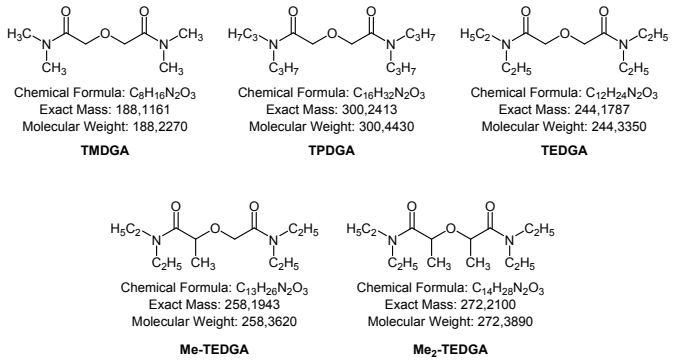

Fig. 1 Chemical structures of the hydrophilic DGAs: *N*,*N*,*N'*,*N'*-tetramethyl diglycolamide (TMDGA), *N*,*N*,*N'*,*N'*-tetrapropyl diglycolamide (TPDGA), *N*,*N*,*N'*,*N'*-tetraethyl diglycolamide (TEDGA), 2-(2-(diethylamino)-2-oxoethoxy)-*N*,*N*-diethyl propanamide (Me-TEDGA), and 2,2'-oxybis(*N*,*N*-diethyl propanamide) (Me_2-TEDGA).

Envisioned large-scale process conditions employ nitric acid (HNO_3) solutions as the aqueous phase, the chemistry of which is drastically different from that of pure water. Previously, TEDGA was found to be susceptible to acid hydrolysis, and other short side-chain DGAs are believed to behave similarly, further limiting their useful lifetime.[16] However, the presence of high solute concentrations of protons (H_{aq}^+) and nitrate anions (NO_3^-) alters the suite of water radiolysis products available for reaction with the hydrophilic DGAs. Both H_{aq}^+ and NO_3^- are efficient scavengers of the hydrated electron (e_{aq}^-, reactions (2) and (3), respectively), and thus capable of completely inhibiting e_{aq}^- reactions with the DGAs.[19] Further, at high acidities there is an appreciable concentration of undissociated HNO_3 ($HNO_3 \rightleftharpoons NO_3^- + H_{aq}^+$, pKa ≈ 1.37)[21], which can scavenge $^\bullet$OH, converting it into the relatively less reactive nitrate radical ($^\bullet NO_3$, E^o = 2.3 – 2.6 V)[22], reaction (5). This is consistent with the reported rate of reaction for TEDGA with the $^\bullet NO_3$, k(TEDGA + $^\bullet NO_3$) = (6.66 ± 0.63) × 10^7 M^{-1} s^{-1}, which is more than an order of magnitude lower than that with the $^\bullet$OH.[16,19,23,24]

$$H_{aq}^+ + e_{aq}^- \rightarrow H^\bullet \qquad k = 2.3 \times 10^{10}\ M^{-1}\ s^{-1} \qquad (2)$$

$$NO_3^- + e_{aq}^- \rightarrow NO_3^{2-} \qquad k = 9.7 \times 10^9\ M^{-1}\ s^{-1} \qquad (3)$$

$$NO_3^- + H^\bullet \rightarrow HNO_3^- \qquad k = 5.6 \times 10^6\ M^{-1}\ s^{-1} \qquad (4)$$

$$HNO_3 + {}^\bullet OH \rightarrow {}^\bullet NO_3 + H_2O \qquad k = 1.9 \times 10^7\ M^{-1}\ s^{-1}. \qquad (5)$$

Further, ionizing radiation energy is partitioned amongst solution components (solutes and solvent molecules) proportional to their electron fraction of the total medium's electron density.[25] In pure water and dilute aqueous solutions, the majority of radiation energy is deposited into the electrons of the water molecules. However, for concentrated HNO_3 solutions (≥1.0 M), an appreciable fraction of radiation energy is partitioned into the electrons of the NO_3^-/HNO_3 molecules, promoting direct generation of additional radiolysis products:[26]

$$NO_3^-/HNO_3 \rightsquigarrow e^-,\ ^\bullet NO_3,\ NO_2^-/HNO_2,\ O,\ H_{aq}^+. \qquad (6)$$

These changes in aqueous phase radiation chemistry may reduce the extent of hydrophilic DGA degradation, leaving acid hydrolysis as their useful lifetime limiting factor. Consequently, the nitrate radiation chemistry of the hydrophilic DGAs needs to be quantitatively established to determine their radiolytic lifetime and viability in the absence of acid hydrolysis.

To this end, we present a systematic investigation into the fundamental radiation chemistry of a series of hydrophilic DGAs in pH neutral, concentrated, aqueous nitrate solutions. An extensive suite of steady-state gamma and time-resolved pulsed electron irradiations, complemented by advanced analytical techniques and predictive multi-scale modelling calculations to provide mechanistic discrimination between radiolytic and hydrolytic effects under envisioned process conditions, is presented.

Experimental

Materials

N,*N*,*N'*,*N'*-tetraethyl diglycolamide (TEDGA, *>99%*), 2-(2-(diethylamino)-2-oxoethoxy)-*N*,*N*-diethyl propanamide (Me-TEDGA, >99%), and 2,2'-oxybis(*N*,*N*-diethyl propanamide (Me_2-TEDGA, >99%) were supplied by Technocomm Ltd. (Wellbrae, Falkland, Scotland, UK). *N*,*N*,*N'*,*N'*-tetrapropyl diglycolamide (TPDGA, >99%) was prepared by Twente University (Enschede, The Netherlands), the synthetic method for which has been previously described.[27] Sodium nitrate ($NaNO_3$, ≥99.995% trace metals basis), potassium thiocyanate (KSCN, ≥99.0% ACS Reagent Grade), *para*-chlorobenzoic acid (pCBA, *99%*), perchloric acid ($HClO_4$, ≥99.999% trace metals basis) potassium phosphate monobasic (99.99% trace metals basis), tertiary-butanol (tBuOH, ≥99.5%), *n*-dodecane (99%), and dichloromethane (DCM, ≥99.8%) were sourced from MilliporeSigma. All chemicals were used without further purification. Ultra-pure water (18.2 MΩ cm) was used to prepare all aqueous solutions. Unless otherwise specified, all solvents for analyses were Merck (Darmstadt, Germany) LC/MS grade or VWR (Darmstadt, Germany) LC/MS grade.

Irradiations

Steady-state. A Shepherd 109-68 cobalt-60 irradiator unit at the Notre Dame Radiation Laboratory (NDRL) was used to perform all steady-state gamma irradiations. Samples consisted of the aforementioned hydrophilic DGAs dissolved in aqueous 5.0 M $NaNO_3$ solutions, irradiated in triplicate as single phases in sealed screw-cap 0.5 dram glass vials to doses up to 200 kGy. TPDGA was not fully soluble in 5.0 M $NaNO_3$ to the desired concentration. Therefore, the stock solution was diluted with water until a clear solution was achieved, with final concentrations of 0.034 M TPDGA and 3.39 M $NaNO_3$. A single set of pure water and *n*-dodecane samples of TPDGA were irradiated under the same conditions for comparison. Dosimetry was determined using Fricke solution,[28,29] subsequently corrected for ^{60}Co decay ($\tau_{1/2}$ = 5.27 years) and solution density, affording an average dose rate of 7.13 kGy h^{-1}.

Time-resolved. Hydrophilic DGA reaction kinetics were determined using the NDRL nanosecond pulsed electron linear accelerator facility and the Brookhaven National Laboratory

(BNL) Laser Electron Accelerator Facility (LEAF). A detailed description of these systems has been given previously.[30-32] Dosimetry was determined using N_2O saturated solutions of 10 mM KSCN at λ_{max} = 470-475 nm ($G_\varepsilon = 5.2 \times 10^{-4}$ m^2 J^{-1}).[33] Isolation and reaction kinetics of specific radicals was achieved using the following conditions:

- *Hydrated electron* (e_{aq}^-). Direct decay kinetics of the e_{aq}^- were observed at 720 nm, using N_2-saturated aqueous solutions of 0.5 M tBuOH and 10 mM phosphate buffer.
- *Hydrogen atom* ($H^\bullet$). pCBA competition kinetics using the direct growth kinetics of the H-pCBA adduct transient absorbance at 370 nm, using N_2-saturated solutions containing 100 µM pCBA, 0.01 M $HClO_4$, and 20 mM tBuOH.
- *Hydroxyl radical* ($^\bullet OH$). KSCN competition kinetics using the direct growth kinetics of the $(SCN)_2^{\bullet-}$ transient observed at 470 nm, using N_2O saturated solutions containing 100 µM KSCN and 10 mM phosphate buffer.
- *Nitrate radical* ($^\bullet NO_3$). Direct decay kinetics of the $^\bullet NO_3$ observed at 630-640 nm using aerated or N_2O-saturated aqueous solutions of 5.0 M $NaNO_3$.
- *Dodecane radical cation ($R^{\bullet+}$).* Direct decay kinetics of $R^{\bullet+}$ were observed at 800 nm, using aerated solutions of 0.5 M DCM in *n*-dodecane.

All transient absorption measurements were made using 1.0 cm optical pathlength quartz cells. TEDGA stock solutions used a flow cell, with flow rate and temperature regulated to ensure that each electron pulse irradiated a fresh sample. Solution temperatures were directly measured by an in-flow thermocouple placed immediately above the irradiation cell. The temperature stability of the system was better than ±0.3 °C. Me-TEDGA, Me_2-TEDGA, and TPDGA irradiations were performed in static cuvettes at ambient room temperature. Kinetic traces were generated through averaging 6–20 individual measurements. Quoted errors for the reaction rate coefficients are a combination of measurement precision and sample concentration errors.

Quantification

Irradiated samples were analyzed at Forschungszentrum Jülich (FZJ) by high performance liquid chromatography – electrospray ionization mass spectrometry/mass spectrometry (HPLC-ESI-MS/MS). The chromatographic separations varied slightly with the DGA analyte. All samples were diluted 1:500,000 and measured in triplicate.

For TEDGA, TPDGA and Me-TEDGA, a Thermo Phenyl-X (100 × 4.6 mm; 2.6 µm particle size) column was used with a gradient of acetonitrile + 0.1% formic acid (A) in 0.1% formic acid in H_2O (B) at 35 °C and a flow-rate of 800 µL min^{-1}. The gradient is described in *Supplementary Information (SI) Table S1* and *Table S2*. Calibration was performed by dilution of unirradiated TEDGA, TPDGA, and Me-TEDGA samples. The linearity was found to be good in the region of 10 to 500 nM with R^2 = 0.9955, 0.9989, and 0.9991, respectively. The variation coefficients of a 100 nM standard were 7.4, 6.0, and 6.2%, respectively. It was found that TPDGA sample dilutions in acetonitrile were unstable, but stable in methanol.

For Me_2-TEDGA, a Phenomenex Luna Omega C18 Polar (100 × 4.6 mm; 2.6 µm particle size) column was used with a gradient of acetonitrile + 0.1% formic acid (A) in 0.1% formic acid in H_2O (B) at 35 °C and a flow-rate of 800 µL min^{-1}. The gradient is described in *SI Table S3*. Calibration was performed by dilution of unirradiated Me_2-TEDGA samples. The linearity was found to be good in the region of 1 to 500 nM with R^2 = 0.9997. The variation coefficient of a 100 nM standard of Me_2-TEDGA was 8.2%.

HPLC-ESI-MS/MS for quantification was performed with a Qtrap6500 instrument (ABSciex, Darmstadt) coupled with an Agilent 1260 HPLC system consisted of a binary pump system, an autosampler and a thermostated column compartment. The MS parameters used for all methods were optimized by performing a Flow Injection Analysis (FIA) with standards and led to the following settings for all analysis: curtain gas (N_2) 40 arbitrary units (a.u.), temperature of the source 350 °C, nebulizer gas (N_2) 40 a.u. and heater gas (N_2) 80 a.u. Quantification after HPLC was performed using ESI-MS/MS detection in the multiple reaction-monitoring (MRM) mode in positive ionization mode. MRM transitions involving precursor ions $(M+H)^+$ and the two most abundant product ions were used for quantification of all analytes as shown in *SI Table S4*. All LC-MS/MS data acquisition and processing was carried out using the *Software Analyst 1.6.1* (AB Sciex, Darmstadt). Quantification was performed with the *Software Multiquant* (AB Sciex, Darmstadt).

Product analysis was performed at FZJ using a hybrid linear ion trap Fourier-Transform Ion Cyclotron Resonance (FTICR) mass spectrometer Linear Tandem Quadrupole Fourier Transform (LTQFT) UltraTM (Thermo Fisher Scientific, Bremen) coupled with an Agilent 1200 HPLC system consisted of a binary pump system, an autosampler, a thermostated column compartment, and a Diode-Array detector (Agilent, Waldbronn). The mass spectrometer was first tuned and calibrated in the positive mode following the standard optimization procedure for all voltages and settings: Source Type: ESI, Ion Spray Voltage: 3.8 kV, Capillary Voltage: 37.00 V, Tube Lens; 130.00 V, Capillary Temp: 275.00 °C, Sheath Gas Flow: 60.00. Mass spectra were recorded in full scan from 100 to 1000 Da with a resolution of 100,000 at *m/z* 400. All data were processed using the *Xcalibur* software version 2.0.

Multi-scale modelling

Kinetic calculations were performed using a multi-scale modelling methodology.[34] A combination of stochastic[35-37] models were used to calculate representative gamma radiation track yields for aerated ($[O_2] = 2.5 \times 10^{-4}$ M) aqueous 3.39 and 5.0 M $NaNO_3$ solutions. Radiation track yields from fits to stochastic data (1.0, 4.0, and 6.0 M $NaNO_{3(aq)}$), in conjunction with nitrate/nitric acid direct effect yields,[38] were used as initial parameters for a deterministic model and solved using the FACSIMILE numerical algorithm (*MCPA software*). For a complete description of this modelling methodology see reference 34. Employed kinetic reaction sets are from water

radiolysis compilations by Buxton *et al.*[19] and Elliot and Bartels[39], a similar nitrate radiolysis reaction scheme as presented in reference 34, and experimental reaction kinetics determined here.

Results and discussion

Reaction kinetics

The kinetic data measured in this study are summarized in Table 1, and corresponding kinetic plots given in *SI*. For comparison purposes, equivalent values for TMDGA are also given.[16] Typical kinetic data is shown in Fig. 2 for the $^{\bullet}OH$ reaction with Me-TEDGA using KSCN competition kinetics.[19]

Table 1 Summary of measured rate coefficients for reaction of the hydrophilic DGAs (TMDGA, TEDGA, Me-TEDGA, Me_2-TEDGA, and TPDGA) with $^{\bullet}OH$, $^{\bullet}NO_3$, $H^{\bullet}$, and e_{aq}^-.

Ligand	Rate coefficient (k, M^{-1} s^{-1})			
	$^{\bullet}OH$ (10^9)	$^{\bullet}NO_3$ (10^8)	$H^{\bullet}$ (10^8)	e_{aq}^- (10^8)
TMDGA[16]	3.06 ± 0.09	3.05 ± 0.12	1.22 ± 0.03	n.d.
TEDGA	2.91 ± 0.10	11.19 ± 0.46	1.60 ± 0.09	2.24 ± 0.10
Me-TEDGA	1.71 ± 0.02	7.79 ± 0.38	0.46 ± 0.06	2.71 ± 0.15
Me_2-TEDGA	1.37 ± 0.02	3.29 ± 0.20	0.36 ± 0.07	0.99 ± 0.08
TPDGA	3.81 ± 0.01	4.83 ± 0.36	0.41 ± 0.02	0.80 ± 0.01

The highest reactivity for these hydrophilic DGAs is seen to be with the $^{\bullet}OH$, of the order of 10^9 M^{-1} s^{-1}. Consistency between the $^{\bullet}OH$ rate coefficients for TEDGA and TMDGA, implies that little $^{\bullet}OH$ reactivity occurs at the C–N alkyl chains; rather, this radical is predominantly reacting with the bridging methylene (-CH_2-) groups. Based upon analogous reactions in the literature,[19] we presume that this reaction occurs by hydrogen atom abstraction from one of these methylene moieties:

$$^{\bullet}OH + TEDGA \rightarrow H_2O + [TEDGA]^{\bullet}. \quad (7)$$

Preference for reaction at these methylene centers can be explained in terms of the carbon centered radical product ($[TEDGA]^{\bullet}$), which is stabilized, relative to radical formation on the C–N alkyl chains, by a combination of electron withdrawal by the ether linkage and delocalization into the carbonyl group. Substitution of these methylene group hydrogen atoms with one (Me-TEDGA) or two (Me_2-TEDGA) methyl groups decreases the $^{\bullet}OH$ rate coefficient. This decrease is attributed to greater steric hindrance imposed by the methyl substituents on this bridging group, impeding the abstraction reaction.

Similar behaviour is observed for $H^{\bullet}$ reactivity with these hydrophilic DGA's, albeit that these reactions occur about an order of magnitude slower than for the $^{\bullet}OH$ reactions. The four extra terminal methylene groups in TEDGA, as compared to TMDGA, facilitate faster hydrogen atom abstraction at these sites:

$$H^{\bullet} + TEDGA \rightarrow H_2 + [TEDGA]^{\bullet}. \quad (8)$$

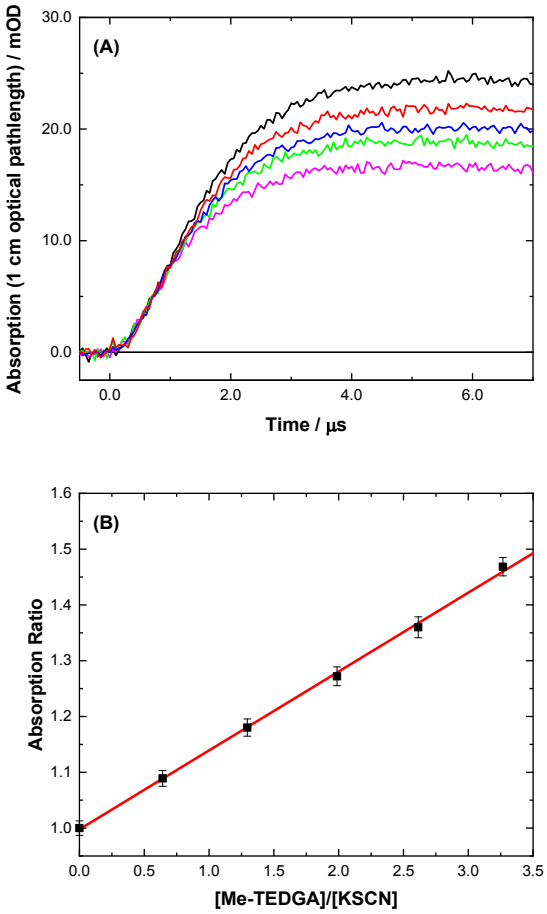

Fig. 2 Determination of the $^{\bullet}OH$ rate coefficient with Me-TEDGA by KSCN competition kinetics. **(A)** Transient growth kinetics are for 98.5 μM KSCN dissolved in N_2O-saturated 10 mM phosphate buffered solution at pH 6.98 and 24.1 °C in the presence of zero (**black**), 63.4 (**red**), 128 (**blue**), 196 (**green**) and 322 (**magenta**) μM added Me-TEDGA. **(B)** Transformed kinetic plot using the peak absorbances of transient kinetics obtained for different Me-TEDGA concentrations. Solid line is a weighted linear fit to transformed data, with a slope of 0.141 ± 0.002, intercept of 0.997 ± 0.005, and R^2 = 0.997, where the slope value corresponds to the second-order reaction rate coefficient for $^{\bullet}OH$ and Me-TEDGA of (1.71 ± 0.02) × 10^9 M^{-1} s^{-1}.

However, the substantial decrease in $H^{\bullet}$ rate coefficient for Me-TEDGA and Me_2-TEDGA again demonstrates that most of the reactivity is at the bridging methylene groups, which have greater steric hindrance and less reactive sites upon methyl-group substitution. Lastly, it would be expected that the TPDGA reaction with this radical would be at least as fast as TEDGA. Unfortunately, this latter measured value is anomalously slower, which we cannot explain at this time.

Based on analogous reactions in the literature,[19] the e_{aq}^- reaction with these DGAs is believed to occur with the carbonyl groups in these molecules:

$$e_{aq}^- + TEDGA \rightarrow [TEDGA]^{\bullet -}. \quad (9)$$

These reactions are slow, but slightly faster than the measured $H^{\bullet}$ reactions. For this radical, the presence of a single methyl group does not appear to significantly impact reactivity. However, having two methyl groups present, as in Me_2-TEDGA,

again provides greater steric hindrance to this reductive process.

The new $^{\bullet}NO_3$ reaction rate coefficients for the methylated TEDGA compounds were considerably faster than TEDGA itself.[16] A re-measurement of this rate coefficient using a new batch of TEDGA gave a much higher rate constant, $(1.12 \pm 0.05) \times 10^9$ M^{-1} s^{-1}, see Table 1 and *SI*. This new value is far more consistent with additional reactivity at the four extra methylene groups in this molecule as compared to TMDGA, with decreasing reactivity shown for the degree of methylation of this molecule, as expected. The reactions between the $^{\bullet}NO_3$ and these hydrophilic DGAs also suggests that the $^{\bullet}NO_3$ is reacting by a combination of both electron and hydrogen atom abstraction:[40]

$$^{\bullet}NO_3 + TEDGA \rightarrow NO_3^- + [TEDGA]^{\bullet+} \quad (10)$$

and

$$^{\bullet}NO_3 + TEDGA \rightarrow HNO_3 + [TEDGA]^{\bullet} \quad (11)$$

The dependence of all these radicals' reaction rate coefficients on the availability of the methylene centers is observed, which presents an opportunity to incorporate radiation resistance/robustness into the design methodology for ligands intended for radiation environments.

Degradation product distribution

The degradation products from irradiated hydrophilic DGAs were identified using HPLC-MS with a high-resolution mass spectrometer, allowing identification of these products by their *m/z* ratios and the corresponding chemical formulae. The intensity of the identified degradation products were followed by measuring the area of the corresponding peaks in the chromatograms when only the *m/z* ratio of the respective degradation product was monitored. Although this method is not precisely quantitative (semi-quantitative), as ionization potentials can be different for different fragments and depend on the total ion count, an estimate of the change in abundance of a product in the samples can be given. The *m/z* ratios of the protonated degradation product ions were used, although usually sodiated product ions, adducts with NH_4^+ ions as well as higher complexes (e.g., 1:2 Na:ligand complexes) were also observed.

The degradation products observed in this study are given in *SI Tables S6* to *S9*, and are generally identical to those observed in previous DGA radiolysis studies.[12-14,16] A schematic representation of possible degradation reactions and the corresponding degradation products is shown in Fig. 3. Comparable to the radiolysis study of hydrophilic DGAs in water,[16] products of single and double de-alkylation reactions, de-amination reactions (with subsequent oxidation to form the carboxylic acid), and O_{ether}–C_{ether} bond breaks were observed. Again, no products of a C_{amide}–C_{ether} bond cleavage could be identified, although such products were observed for lipophilic DGAs with low abundance.[12-14]

The alcohols formed through O_{ether}–C_{ether} bond cleavage were identified in all irradiated samples. For Me-TEDGA two different products can be formed, depending on which of the

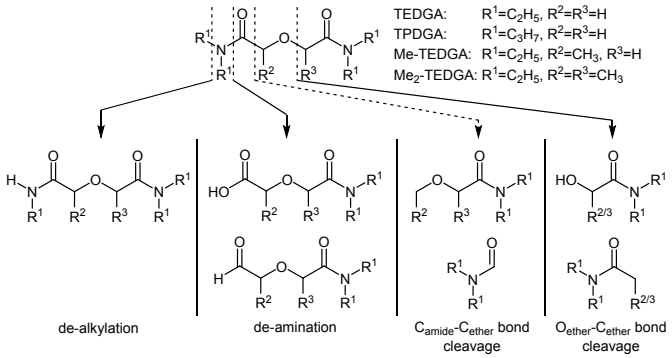

Fig. 3 Schematic representation of possible degradation reactions and corresponding degradation products.

two different O_{ether}–C_{ether} bonds are broken. In this study, we observed that the degradation product of the unsubstituted O_{ether}–C_{ether} bond break is present in much higher intensity (ca. 20-times higher intensities). Additionally, the reaction products of the single de-alkylation and the alcohol radical formed by O_{ether}–C_{ether} bond cleavage (see Fig. 4) were detected with the product deriving from the unsubstituted O_{ether}–C_{ether} bond break again being found in higher intensity. Therefore, we assume that the methyl-substituted O_{ether}–C_{ether} bond reacts slower with the primary radicals from solvent radiolysis

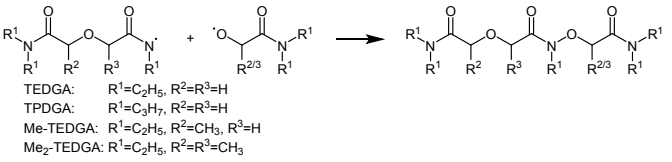

Fig. 4 Reaction scheme of the combination reaction of the single de-alkylation product radical with the alcohol radical formed by O_{ether}–C_{ether} bond cleavage.

(although the overall degradation rate of the molecule may be less affected). These observations are consistent with our rate coefficient trends, and has been previously postulated for the lipophilic analogue of Me-TEDGA.[14]

Addition products of the hydrophilic DGAs with radiolytic NO_x species (e.g., NO, $^{\bullet}NO_3$, and $^{\bullet}NO_2$) were also observed. Interestingly, for the unsubstituted TEDGA and TPDGA molecules mainly NO and NO_2 adducts were detected, while NO_3 adducts were seen only with little intensity. All three NO_x addition products were observed for Me-TEDGA and Me_2-TEDGA. Similar reaction products of radiolytic NO_x species with the single de-alkylation products were also measured.

Overall, similar product distributions were observed for the radiation-induced degradation of the hydrophilic DGAs in concentrated $NaNO_{3(aq)}$ as in pure water conditions, indicating similar radiolytic pathways. However, in concentrated $NaNO_{3(aq)}$ solutions, reaction products with radiolytic NO_x species are observed. These addition products may have metal complexing ability of their own, and thus may have more significant impact upon separation process performance than those degradation products formed under pure water conditions alone. These NO_x adducts need to be isolated and their respective chemistries elucidated.

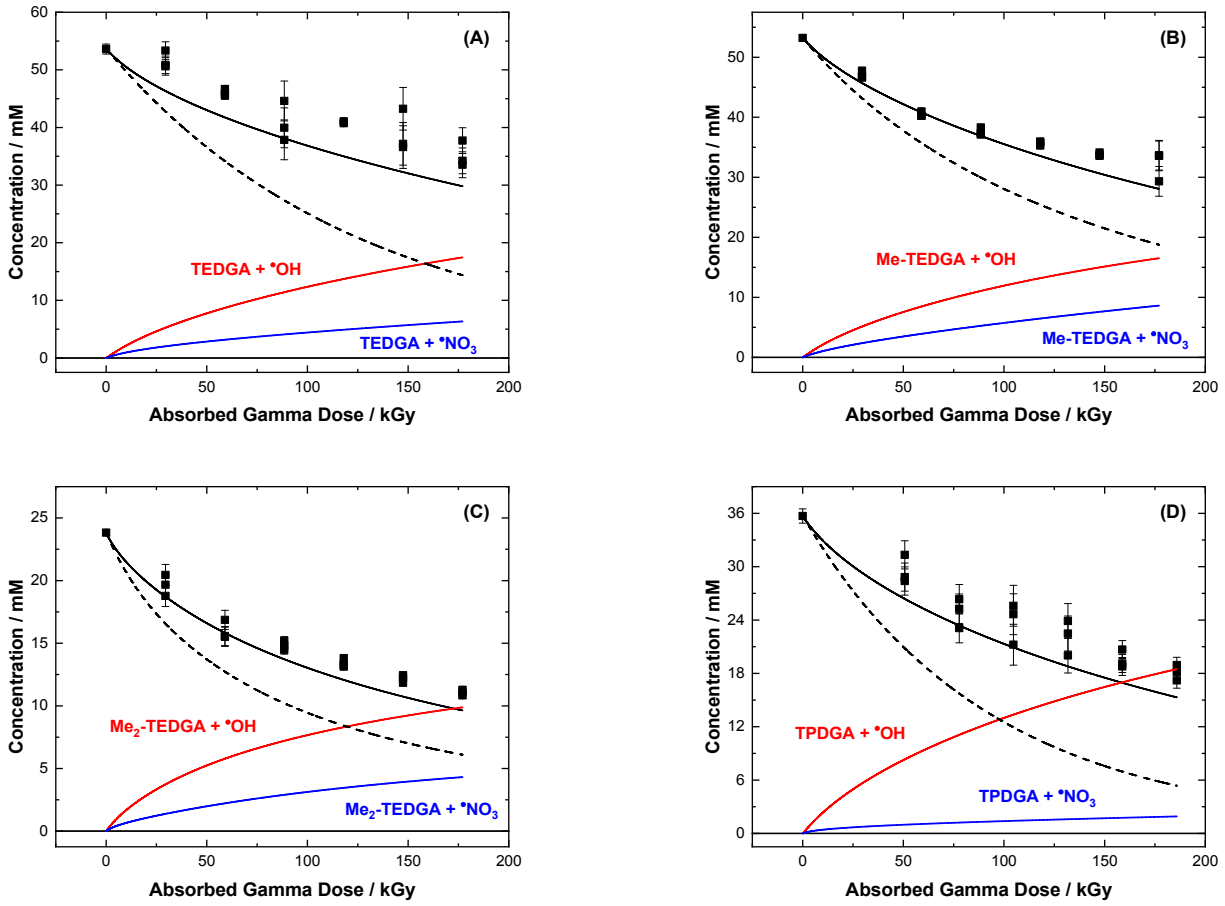

Fig. 5 Gamma radiolysis of hydrophilic DGAs in concentrated, aqueous nitrate solution as a function of absorbed dose: (A) TEDGA; (B) Me-TEDGA; (C) Me_2-TEDGA; and (D) TPDGA. Curves are from multi-scale calculations predicting DGA decay without secondary degradation product reactions (**dashed black**) and with secondary degradation product reactions (**solid black**) and corresponding accumulated reaction kinetics for •OH (**red**) and $•NO_3$ (**blue**).

Ligand degradation rates

The measured and calculated rates of gamma-induced radiolytic degradation of TEDGA, Me-TEDGA, Me_2-TEDGA, and TPDGA in concentrated, aqueous nitrate solution are shown in Fig. 5. All four molecules are susceptible to gamma radiolysis and exhibit first order decay with increasing absorbed dose, the dose constants for which are given in Table 2.[18] As with their lipophilic analogues, the hydrophilic DGA dose constants in concentrated, aqueous nitrate solution are relatively insensitive to alkyl substitution, affording an average value of (-3.18 ± 0.23) × 10^{-6} Gy^{-1}. The average hydrophilic DGA dose constant is much lower than the complimentary dose constants reported for pure water.[16] This is indicative of significant differences in radiation chemistry between the two systems. As previously discussed, the presence of concentrated nitrate significantly alters the available radiolytic species for reaction with the hydrophilic DGAs. Multi-scale calculations presented in Fig. 5 show that radiolytic degradation is driven by reaction with the •OH and, to a lesser extent, the $•NO_3$, which is consistent with their kinetics in Table 1. Reaction of the hydrophilic DGAs with the •OH was invoked to predominantly explain their rate of degradation under pure water conditions.[16]

Table 2 Pseudo-first-order dose constants for the gamma irradiation of TEDGA, Me-TEDGA, Me_2-TEDGA, and TPDGA under pure water and concentrated, aqueous nitrate conditions.

Hydrophilic DGA	**Dose constant** (× 10^{-6} Gy^{-1})	
	Pure water	Concentrated aqueous nitrate
TEDGA	-10.3 ± 1.13[16]	-2.36 ± 0.25
Me-TEDGA	-7.8 ± 0.7[16]	-2.93 ± 0.17
Me_2-TEDGA	-7.3 ± 2.1[16]	-3.90 ± 0.21
TPDGA	-8.39 ± 0.29	-3.54 ± 0.29

However, the differences between dose constants for pure water and concentrated, aqueous nitrate must be due to:

1. Chemistries associated with the reducing products of water radiolysis (i.e., the e_{aq}^- and the H•). In concentrated,

aqueous nitrate solutions, there is negligible contribution from the e_{aq}^- and H•, as both are rapidly scavenged by NO_3^- within the lifetime of the radiation chemical track; reactions (3) and (4).

2. Reduced reactivity of the •NO_3 relative to the •OH, which is clear from the measured rate coefficients given in Table 1. In addition to reactivity differences, the •NO_3 rate coefficients exhibit less selectivity for the methylene sites, which may provide some explanation as to why the hydrophilic DGA dose constants are less sensitive to alkyl substitution under concentrated, aqueous nitrate conditions compared with pure water conditions.

Agreement between experiment and calculation was achieved by the incorporation of additional •OH and •NO_3 reactions with degradation products from hydrophilic DGA radiolysis. The importance of these secondary scavenging processes has been recently highlighted by Horne *et al.* for similarly aqueous miscible sulfonated bis-triazinyl-bipyridine ligands,[41] and is clearly demonstrated by comparison of calculations with (**solid black**) and without (**dashed black**) secondary degradation product scavenging reactions in Fig. 5. In their absence, multi-scale calculations predict a faster rate of DGA degradation than is observed. This demonstrates that certain degradation products (e.g., the alcohol species shown in Fig. 3) accumulate and compete for the oxidizing radical species, in turn reducing the extent to which they react with the parent DGA compounds. In the absence of a comprehensive study of the radiolytic behaviour of all identified degradation products, presented multi-scale calculations employ a simple degradation product (DP) scavenging reaction with an optimized rate coefficient to achieve agreement with experiment:

$$\text{DGA DP} + {}^{\bullet}\text{OH}/{}^{\bullet}\text{NO}_3 \rightarrow \text{Other products.} \quad (12)$$

However, this does not preclude these steady-state radiolysis products (e.g., hydrogen peroxide and the nitrite anion) from being involved in radical capping processes.

Overall, the presence of concentrated, aqueous nitrate significantly reduces the rate of hydrophilic DGA degradation, relative to pure water. When hydrophilic and lipophilic DGA dose constants are compared in Fig. 6, we can see that the radiation robustness of the hydrophilic DGAs in concentrated, aqueous nitrate solution is similar to that of their lipophilic analogues. This is most clearly demonstrated by TPDGA (301.5 g mol^{-1}), which is soluble in both aqueous and organic media, and found to react with $R^{\bullet+}$ with a rate coefficient of (6.18 ± 0.39) × 10^{10} M^{-1} s^{-1}:

$$R^{\bullet+} + \text{TPDGA} \rightarrow R + [\text{TPDGA}]^{\bullet+}. \quad (13)$$

The similarity between concentrated, aqueous nitrate and organic media DGA dose constants is most promising for large-scale separation process applications and indicates that in the presence of concentrated nitrate, acid hydrolysis, not radiolysis, will limit their useful lifetime. Complementary nitric acid radiolysis studies are underway to further evaluate the potential of these hydrophilic DGAs.

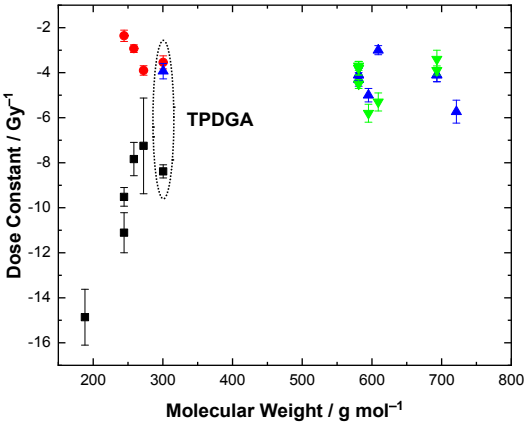

Fig. 6 Hydrophilic and lipophilic DGA gamma radiolysis dose constants as a function of molecular weight and solvent formulation: pure water (■, this work and reference 16), 5.0 and 3.39 M $NaNO_{3(aq)}$ (●, this work), *n*-dodecane (▲, this work and references 12, 13, 14, and 16), and *n*-dodecane/$HNO_{3(org)}$ (▼, references 12, 13, and 14).

Conclusions

Hydrophilic DGAs are promising actinide and lanthanide stripping and hold-back agents, although their useful lifetime is constrained by water radiolysis and nitric acid hydrolysis – both are significant factors under expected large-scale separation process conditions. However, the speciation of problematic primary water radiolysis products (i.e., e_{aq}^-, •H, and •OH) is significantly different under concentrated nitrate/nitric acid conditions.

To discriminate between radiolytic and hydrolytic effects, the irradiation of a series of hydrophilic DGAs (TEDGA, Me-TEDGA, Me_2-TEDGA, and TPDGA) in concentrated, aqueous nitrate solution, has shown that the rate of radiolytic degradation is significantly reduced, relative to pure water conditions. Further, their radiation-induced decay affords an average dose constant ((-3.18 ± 0.23) × 10^{-6} Gy^{-1}) similar to that of their lipophilic analogues, many of which have been successfully employed in scaled-up separation processes.

Multi-scale calculations, supported by experimental reaction kinetics and degradation product distribution measurements, have demonstrated that hydrophilic DGA degradation in the presence of concentrated, aqueous nitrate is driven by •OH and, to a lesser extent, •NO_3 oxidation, as the reducing products of water radiolysis are inhibited by NO_3^- scavenging. Further, net DGA decomposition is progressively inhibited by reaction of their own degradation products with the •OH and the •NO_3. Consequently, we can expect for acid hydrolysis, not radiolysis, to limit their useful lifetime, especially in concentrated HNO_3 solutions, where the •NO_3 is the predominant oxidant due to •OH scavenging by HNO_3.

Conflicts of interest

There are no conflicts to declare.

Acknowledgements

This research has been funded by the US Department of Energy (US-DOE) Assistant Secretary for Nuclear Energy, under the Fuel Cycle Research & Development Radiation Chemistry program; DOE-Idaho Operations Office Contract DE-AC07-05ID14517 and Nuclear Energy Universities Program (NEUP) DE-NE0008406 grant.

The time-resolved pulsed electron irradiations reported herein were performed at: the Notre Dame Radiation Laboratory, supported by the Division of Chemical Sciences, Geosciences and Biosciences, Basic Energy Sciences, Office of Science, US-DOE through Award No. DE-FC02-04ER15533; and the Brookhaven National Laboratory (BNL) Laser Electron Accelerator Facility of the BNL Accelerator Center for Energy Research, supported by the US-DOE Office of Basic Energy Sciences, Division of Chemical Sciences, Geosciences, and Biosciences under contract DE-SC0012704.

All gamma irradiation analyses were performed at Forschungszentrum Jülich, with financial support from the European Commission through the Safety of Actinide Separation Processes (SACSESS) project, under contract No. FP7-Fission-2012-323-282, and the European GEN IV Integrated Oxide Fuels Recycling Strategies (GENIORS) project, grant agreement No. 730227.

Notes and references

(1) R. Taylor, Reprocessing and Recycling of Spent Nuclear Fuel, First. ed.; Woodhead Publishing: Oxford, 2015.
(2) D. Whittaker, A. Geist, G. Modolo, R. Taylor, M. Sarsfield and A. Wilden, *Solvent Extr. Ion Exch.*, 2018, **36**, 223.
(3) S. A. Ansari, P. Pathak, P. K. Mohapatra and V. K. Manchanda, *Chem. Rev.*, 2012, **112**, 1751.
(4) C. Musikas and H. Hubert, *Solvent Extr. Ion Exch.*, 1987, **5**, 877.
(5) S. Chapron, C. Marie, G. Arrachart, M. Miguirditchian and S. Pellet-Rostaing, *Solvent Extr. Ion Exch.*, 2015, **33**, 236.
(6) S. Chapron, C. Marie, V. Pacary, M. T. Duchesne, G. Arrachart, S. Pellet-Rostaing and M. Miguirditchian, *Procedia Chem.*, 2016, **21**, 133.
(7) L. Klaß, A. Wilden, F. Kreft, C. Wagner, A. Geist, P. J. Panak, I. Herdzik-Koniecko, J. Narbutt and G. Modolo, G., *Solvent Extr. Ion Exch.*, 2019, **37**, 297.
(8) Y. Sasaki, Y. Sugo, Y. Kitatsuji, A. Kirishims, T. Kimura and G. R. Choppin, *Anal. Sci.*, 2007, 23, 727.
(9) G. J. Lumetta, A. V. Gelis, J. C. Carter, C. M. Niver and M. R. Smoot, *Solvent Extr. Ion Exch.*, 2014, 32, 333.
(10) C. Rostaing, C. Poinssot, D. Warin, P. Baron and B. Lorrain, *Procedia Chem.*, 2012, **7**, 367.
(11) S. Lange, A. Wilden, G. Modolo, F. Sadowski, M. Gerdes and D. Bosbach, *Solvent Extr. Ion Exch.*, 2017, **35**, 161.
(12) C. A. Zarzana, G. S. Groenewold, B. J. Mincher, S. P. Mezyk, A. Wilden, H. Schmidt, G. Modolo, J. F. Wishart and A. R. Cook, *Solvent Extr. Ion Exch.*, 2015, **33**, 431.
(13) K. M. Roscioli-Johnson, C. A. Zarzana, G. S. Groenewold, B. J. Mincher, A. Wilden, H. Schmidt, G. Modolo and B. Santiago-Schubel, *Solvent Extr. Ion. Exch.*, 2016, **34**, 439.
(14) H. Galan, C. A. Zarzana, A. Wilden, A. Nunez, H. Schmidt, R. J. M. Egberink, A. Leoncini, J. Cobos, W. Verboom, G. Modolo, G. S. Groenewold and B. J. Mincher, *Dalton Trans.*, 2015, **44**, 18049.
(15) Y. Sugo, Y. Izumi, Y. Yoshida, S. Nishijima, Y. Sasaki, T. Kimura, T. Sekine and H. Kudo, *Radiat. Phys. Chem.*, 2007, **76**, 794.
(16) A. Wilden, B. J. Mincher, S. P. Mezyk, L. Twight, K. M. Rosciolo-Johnson, C. A. Zarzana, M. E. Case, M. Hupert, A. Stärk and G. Modolo, *Solvent Extr. Ion Exch.,* 2018, **36**, 347.
(17) T. Koubsky and J. Lustinec, *J. Radioanal. Nucl. Chem.* 2018, **318**, 2407.
(18) B. J. Mincher and R. D. Curry, *Appl. Rad. Isot.*, 2000, **52**, 189.
(19) G. V. Buxton, C. L. Greenstock, W. P. Helman and A. B. Ross, *J. Phys. Chem. Ref. Data*, 1988, **17**, 513.
(20) Y. Yoshida, T. Ueda, T. Kobayashi, H. Shibata and S. Tagawa, *Nucl. Inst. Meth. Phys. Res. A*, 1993, **327**, 41.
(21) W. Davis and H. J. De Bruin, *J. Inorg. Nucl. Chem.*, 1964, **26**, 1069.
(22) P. Y. Jiang, Y. Katsumura, K. Ishigure and Y. Yoshida, *Inorg. Chem.*, 1992, **31**, 5135.
(23) S. P. Mezyk and D. M. Bartels, *J. Phys. Chem. A*, 1997, **101**, 6233.
(24) T. Logager and K. Sehested, *J. Phys. Chem.*, 1993, **97**, 6664.
(25) A. J. Swallow and M. Inokuti, *Radiat. Phys. Chem.*, 1988, **32**, 185.
(26) Y. Katsumura, The Chemistry of Free Radicals: N-Centered Radicals, John Wiley & Sons, Chichester, 1998.
(27) A. leoncini, J. Huskens and W. Verboom, *Synlett*, 2016, **27**, 2463.
(28) H. Fricke and E. J. Hart, *J. Chem. Phys.*, 1935, **3**, 60.
(29) N. F. Barr and R. H. Schuler, *J. Phys. Chem.*, 1959, **63**, 808.
(30) K. Whitman, S. Lyons, R. Miller, D. Nett, P. Treas, A. Zante, R. W. Fessenden, M. D. Thomas and Y. Wang, Linear Accelerator for Radiation Chemistry Research at Notre Dame. *Proceedings of the '95 Particle Accelerator Conference and International Conference on High Energy Accelerators*, Texas, USA. 1996.
(31) G. L. Hug, Y. Wang, C. Schöneich, P. Y. Jiang and R. W. Fessenden, *Radiat. Phys. Chem.*, 1999, **54**, 559.
(32) J. F. Wishart, A. R. Cook and J. R. Miller, *Rev. Sci. Instrum.*, 2004, **75**, 4359.
(33) G. V. Buxton and C. R. Stuart, *J. Chem. Soc. Faraday Trans.*, 1995, **92**, 279.
(34) G. P. Horne, T. A. Donoclift, H. E. Sims, R. M. Orr and S. M. Pimblott, *J. Phys. Chem. B*, 2016, **120**, 11781.
(35) S. M. Pimblott, J. A. LaVerne and A. Mozumder, *J. Phys. Chem.*, 1996, **100**, 8595.
(36) S. M. Pimblott and J. A. LaVerne, *J. Phys. Chem. A*, 2002, **106**, 9420.
(37) P. Clifford, N. J. B. Green, M. J. Oldfield, M. J. Pilling and S. M. Pimblott, *J. Chem. Soc., Faraday Trans.*, 1986, **82**, 2673.
(38) P. Y. Jiang, R. Nagaishi, T. Yotsuyanagi, Y. Katsumura and K. Ishigure, *J. Chem. Soc. Faraday Trans.*, 1994, **90**, 93.
(39) A. J. Elliot and D. M. Bartels, The Reaction Set, Rate Constants and G-Values for the Simulation of the Radiolysis of Light Water Over the Range 20° to 350°C Based on Information Available in 2008. AECL Nuclear Platform Research and Development – Report 153-127160-450- 001. 2009.
(40) S. P. Mezyk, T. D. Cullen, K. A. Rickman and B. J. Mincher, *Int.*

J. Chem. Kin., 2017, **49**, 635.
(41) G. P. Horne, S. P. Mezyk, N. Moulton, J. R. Peller and A. Geist, A. *Dalton Trans.*, 2019, **48**, 4547.